Archival Report

Biological Psychiatry

Retraction of Astrocyte Leaflets From the Synapse Enhances Fear Memory

Aina Badia-Soteras, Tim S. Heistek, Mandy S.J. Kater, Aline Mak, Adrian Negrean, Michel C. van den Oever, Huibert D. Mansvelder, Baljit S. Khakh, Rogier Min, August B. Smit, and Mark H.G. Verheijen

ABSTRACT

BACKGROUND: The formation and retrieval of fear memories depends on orchestrated synaptic activity of neuronal ensembles within the hippocampus, and it is becoming increasingly evident that astrocytes residing in the environment of these synapses play a central role in shaping cellular memory representations. Astrocyte distal processes, known as leaflets, fine-tune synaptic activity by clearing neurotransmitters and limiting glutamate diffusion. However, how astroglial synaptic coverage contributes to mnemonic processing of fearful experiences remains largely unknown.

METHODS: We used electron microscopy to observe changes in astroglial coverage of hippocampal synapses during consolidation of fear memory in mice. To manipulate astroglial synaptic coverage, we depleted ezrin, an integral leaflet-structural protein, from hippocampal astrocytes using CRISPR (clustered regularly interspaced short palindromic repeats)/Cas9 gene editing. Next, a combination of Föster resonance energy transfer analysis, genetically encoded glutamate sensors, and whole-cell patch-clamp recordings was used to determine whether the proximity of astrocyte leaflets to the synapse is critical for synaptic integrity and function.

RESULTS: We found that consolidation of a recent fear memory is accompanied by a transient retraction of astrocyte leaflets from hippocampal synapses and increased activation of NMDA receptors. Accordingly, astrocyte-specific depletion of ezrin resulted in shorter astrocyte leaflets and reduced astrocyte contact with the synaptic cleft, which consequently boosted extrasynaptic glutamate diffusion and NMDA receptor activation. Importantly, after fear conditioning, these cellular phenotypes translated to increased retrieval-evoked activation of CA1 pyramidal neurons and enhanced fear memory expression.

CONCLUSIONS: Together, our data show that withdrawal of astrocyte leaflets from the synaptic cleft is an experience-induced, temporally regulated process that gates the strength of fear memories.

https://doi.org/10.1016/j.biopsych.2022.10.013

Remembering experiences that involve fear, pain, or trauma may lead to the development and progression of psychopathologies, such as depression, anxiety, posttraumatic stress disorder, and substance abuse (1). Preclinical and clinical evidence has revealed that the hippocampus and the amygdala, among other regions, are key brain structures associated with maladaptive responses that underlie these psychiatric disorders (2–4). In particular, coordinated activity of hippocampal neuronal ensembles is thought to be critical in the formation and expression of the contextual information of recently acquired aversive memories (5–7). Converging evidence over the past years indicates that changes in the structural and/or physiological properties of synapses, including interactions with their perisynaptic environment, are required for the formation, storage, and retrieval of recent memories (8–11). Thus, decoding the molecular and cellular framework that supports memory processes is of the utmost importance for understanding memory-related disorders.

Recently, evidence has emerged that hippocampal astrocytes are implicated in the formation and remodeling of aversive memories and stress-related disorders (12–16). For example, activation of the Gq-coupled receptor hM3Dq in CA1 astrocytes during fear conditioning enhanced recent fear memory (12), whereas activation of the Gi-coupled receptor hM4Di impaired remote recall (13). Thus, it is evident that hippocampal-dependent memory processing of aversive events requires coordinated activity of astrocytes and neurons.

Astrocytes are morphologically complex glial cells that contact synapses with their thinnest terminal processes, referred to as leaflets or perisynaptic astrocyte processes, which together with pre- and postsynaptic neuronal elements are an integral feature of synapses throughout the central nervous system (17–19). Astrocytic leaflets fine-tune local synaptic transmission and plasticity because they are ideally positioned proximally to the synaptic cleft (20) and contain the

ISSN: 0006-3223

molecular machinery to modulate the extracellular space around synapses (21,22). Astrocyte leaflets are enriched in actin-associated proteins of the ERM (ezrin radixin moesin) family (23) that dynamically regulate astrocytic filopodia formation in culture (24) and astrocyte morphogenesis in the developing somatosensory cortex (25). Changes in the astroglial coverage of synapses have been observed in vivo in the hypothalamus during lactation (26,27) and sleep/awake cycles (28), in the nucleus accumbens after self-administered psychostimulants (29–31), and in the lateral amygdala following threat conditioning (32). Similarly, synaptic activity and synaptic potentiation has been reported to induce remodeling of astrocytic leaflets on a short time scale (30–60 minutes after stimulation) in the hippocampus (33–37). However, these studies were performed in fixed and acute slices, and whether this structural plasticity of astrocytic leaflets occurs in vivo and on a longer timescale (hours to days), such as in long-term memory processing, is an important and intriguing question that remains to be addressed. Accordingly, the question of whether astrocytic ezrin is required for the structural and functional integrity of hippocampal synapses and memory processes has remained unexplored.

To this end, we examined astrocyte leaflet-synapse spatial interaction in the hippocampus during the formation and consolidation of fear memories and found a learning-induced transient retraction of astrocyte leaflets. Altogether, our data reveal that the apposition of astrocyte leaflets to the synaptic cleft influences contextual fear memory expression and gates neuronal activation in a context-dependent manner.

METHODS AND MATERIALS

Description of additional methods are available in the Supplement.

Animals

Wild-type, male C57BL/6J mice were 8 to 10 weeks old at the start of experiments and were individually housed on a 12-hour light/dark cycle with ad libitum access to food and water. Behavioral experiments were performed during the light phase. All experimental procedures were approved by the Netherlands Central Committee for Animal Experiments and the Animal Ethical Care Committee of the Vrije Universiteit Amsterdam (AVD1120020174287). Mice were randomly assigned to experimental groups.

Constructs

The pAAV- GfaABC$_1$D::Cas9-HA-Ezr was generated by first replacing the cytomegalovirus promoter from pX601-AAV-CMV::NLS-saCas9-NLS-3xHA-bGHpA;Bsal-sgRNA (Addgene plasmid No. 61591) with the GFAP promoter (GfaABC$_1$D). Next we inserted the designed single guide RNA (sgRNA) to target exon-1 of *Ezr* (TGGCTGGTTGGTGGCTCTGCGTGGGT, GenScript: NM_001271663.1_T3; CCGTCGCCTCCGCCGTACAGCCGAAT, GenScript: NM_001271663.1_T2). Finally, we cloned the modified plasmid to an AAV2/5 vector. The control virus, pAAV- GfaABC$_1$D::Cas9-HA, was generated following the same procedure, but it lacks the sequence to target *Ezr*.

Neuron-Astrocyte Proximity Assay and Föster Resonance Energy Transfer Analyses

Föster resonance energy transfer (FRET) from acute slices was examined 4 to 6 weeks following AAV (adeno-associated virus) injections in vivo. We measured FRET by sensitized emission using PixFRET, an ImageJ plug-in. Image processing was carried out as described previously (38).

RESULTS

Contextual Fear Learning Causes Transient Retraction of Astrocyte Leaflets From the Synaptic Cleft

We first assessed the spatial organization of astrocyte leaflets in apposition to the synaptic elements after contextual fear conditioning (CFC). Mice underwent CFC, and astroglial synaptic coverage was determined using electron microscopy (EM) in the CA1 at successive time points 30 minutes, 5 days, and 28 days after training (Figure 1A). Mice that remained in their home cage (HC) were used as controls. The number of synapses without astrocyte contact (no contact) (Figure 1B) and synapses contacted by an astrocyte leaflet (only postsynapse, only presynapse, and both) (Figure 1B) did not differ between time points (Figure 1B). Also, compared with HC control mice, the extent of astrocyte contact with the pre- and postsynapse (Figure S1A, B), as well as the perimeter of both synaptic structures (Figure S1C, D), was unaltered during encoding and consolidation (30 minutes and 5 days). A decrease in postsynapse-leaflet contact was found at the remote time point (28 days) (Figure S1B), which is likely related to the observed increased spine size (Figure S1D) because astroglial synapse coverage is inversely correlated with spine size (39). Importantly, and consistent with the notion that encoding and retrieval of recent contextual memories are mediated by the hippocampus (6,40), we observed a rapid (30 minutes) and persistent (5 days) shortening of astrocyte leaflets following CFC that was no longer present at a remote time point (28 days) (Figure 1C, E; Figure S1E–G). These observations were complemented by an increased distance of the astrocyte leaflet to the synaptic cleft at 30 minutes and 5 days after CFC (Figure 1D, E; Figure S1H–J). To examine whether the changes in astrocyte coverage were specific to associative learning, we analyzed a group at 5 days after immediate shock (IS) exposure (IS 5d). We found that the IS 5d group exhibited a slightly shorter leaflet tip than the HC control, whereas no differences were observed for the astrocyte leaflet distance to the synaptic cleft (Figure S1K, L). It is important to note that although there is a significant reduction of the astrocyte leaflet tip after IS, this difference is minor (8 nm, 13% of HC) (Figure S1K) compared with the change observed 5 days after CFC (17 nm, 25% of HC) (Figure 1C), indicating that the stress of an aversive stimulus and/or exposure to a new context may cause minor changes in the leaflet tip length; however, this is not sufficient to cause a detectable increase in the distance of the leaflet tip from the synaptic cleft. Taken together, encoding and consolidation of contextual fear memory is accompanied by a transient retraction of astrocyte leaflets from the synaptic cleft.

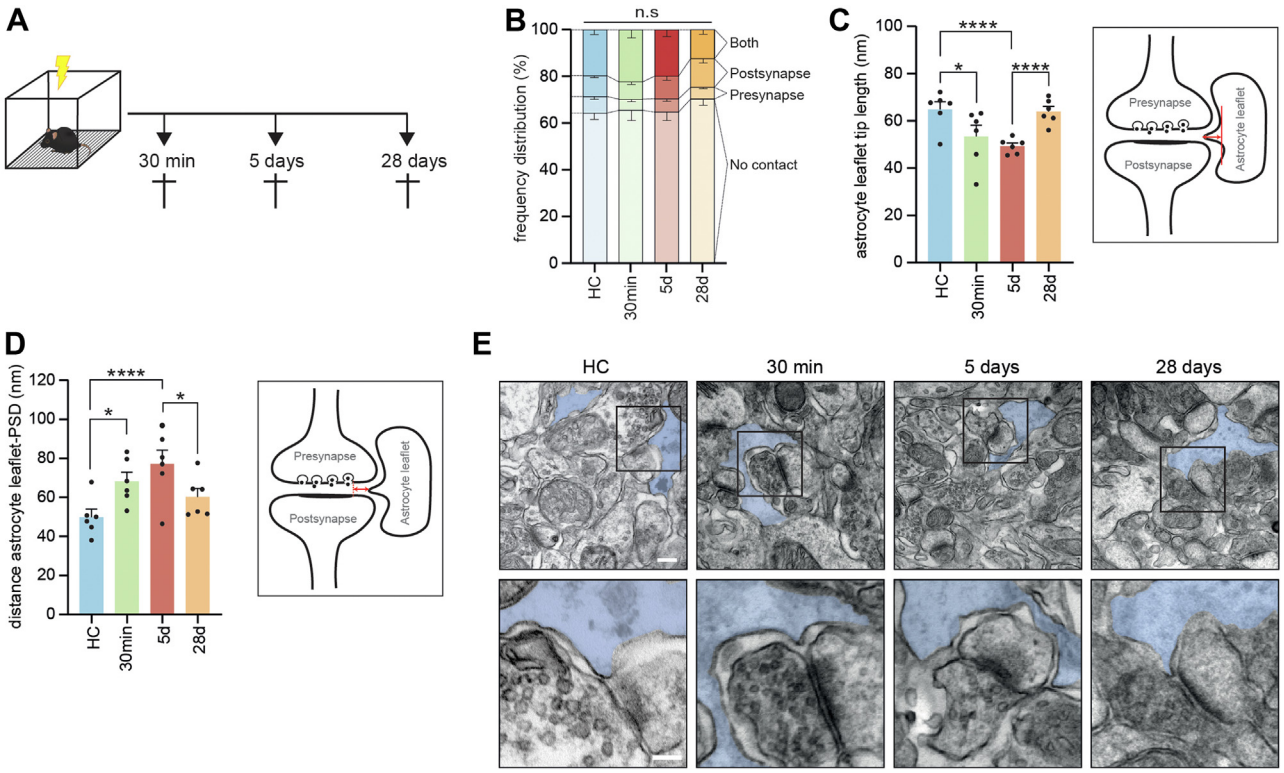

Figure 1. CFC induces transient retraction of the astrocyte leaflet from the synaptic cleft. **(A)** Experimental workflow: mice were sacrificed 30 minutes, 5 days, and 28 days after conditioning. HC mice were used as controls. **(B)** Frequency distributions for the different types of astrocyte leaflet-synapse contact: synapse without an astrocyte contact (no contact), astrocyte leaflet contacts only the presynaptic button (presynapse), astrocyte leaflet contacts only the postsynapse spine (postsynapse), and astrocyte leaflet contacts both synaptic elements (both) at the depicted time points after CFC. $\chi^2_{9,742} = 4.77$, $p = .85$; n.s. **(C)** (Left) Quantification of astrocyte leaflet tip length at the depicted time points after CFC (HC: 130 synapses from 6 mice; 30 minutes: 152 synapses from 6 mice; 5 days: 123 synapses from 6 mice; 28 days: 86 synapses from 6 mice); $F_{3,487} = -11.6$, $p < .0001$ post hoc Bonferroni test: HC vs. 30 minutes $^*p = .01$, HC vs. 5 days $^{****}p < .0001$, HC vs. 28 days $p = .99$, 30 minutes vs. 5 days $p = .07$, 30 minutes vs. 28 days $p = .06$, 5 days vs. 28 days $^{****}p < .0001$. (Right) Illustration depicting how the length of the astrocyte leaflet tip is measured. **(D)** (Left) Quantification of astrocyte leaflet distance from the PSD at depicted time points after CFC (HC: 122 synapses from 6 mice, 30 minutes: 142 synapses from 6 mice, 5 days: 133 synapses from 6 mice, 28 days: 80 synapses from 6 mice); $F_{3,117} = -9.32$, $p < .0001$ post hoc Bonferroni test: HC vs. 30 minutes $^*p = .01$, HC vs. 5 days $^{****}p < .0001$, HC vs. 28 days $p = .41$, 30 minutes vs. 5 days $^*p = .15$, 30 minutes vs. 28 days $p = .62$, 5 vs. 28 days $^*p = .01$. (Right) Illustration depicting how the astrocyte leaflet distance from the PSD is measured. **(E)** Representative images of astrocyte leaflet-synapse interaction during fear memory processing. In light purple, an astrocyte leaflet contacting an excitatory synapse is depicted. Scale bar = 200 nm (top row) and 100 nm (bottom row). Data are presented as mean ± SEM. CFC, contextual fear conditioning; HC, home cage; n.s., not significant; PSD, postsynaptic density.

Structural Manipulation of Astrocyte Leaflets by CRISPR/Cas9-Mediated Depletion of Ezrin

To mimic the changes in leaflet structure observed using EM and to subsequently study synaptic function and behavior in vivo, we specifically reduced ezrin expression in CA1 astrocytes of adult mice by delivering an AAV vector (AAV2/5) encoding the saCas9 enzyme under the control of the minimal astrocyte-specific GFAP promoter and a sgRNA complementary to *Ezr* (exon-1), (AAV2/5-GfaABC$_1$D::Cas9-HA-Ezr) (Figure 2A). Stereotaxic delivery of this vector was restricted to dorsal CA1 astrocytes (Figure S2A, B), with high transduction efficiency (82.7 ± 2.9% [mean ± SEM] of astrocytes expressing Cas9) and very high specificity (Figure 2B, C). Next we examined ezrin levels by combining RNA scope in situ hybridization and immunofluorescence analysis 4 to 5 weeks after AAV delivery. We found strong reduction (72%) in ezrin RNA levels in the dorsal CA1 of mice expressing saCas9 together with the sgRNA against ezrin (Ezr-saCas9) compared with control mice expressing only saCas9 (control: 27.4 ± 2.7, Ezr-saCas9: 7.5 ± 1.2 RNA molecules per astrocyte) (Figure 2D, E). Similarly, ezrin protein levels were found to be reduced in Ezr-saCas9 mice compared with control mice (Ezr-saCas9: 27.1 ± 5.7% ezrin signal arbitrary units relative to control) (Figure 2F, G). To determine possible virus-induced reactive astrogliosis (41), we investigated the number of astrocytes and GFAP protein levels but did not find signs of astrogliosis (Figure S2C–E). Thus, the current approach enabled us to optimally and selectively reduce *Ezr* expression in a large population of hippocampal astrocytes and to bypass any developmental role of this protein.

Astrocyte Morphological Complexity and Astrocyte-Neuron Proximity Are Decreased in the Hippocampus After *Ezr* Deletion

Next we determined whether ezrin indeed shapes astrocyte morphology and astrocyte-neuron contacts in the adult

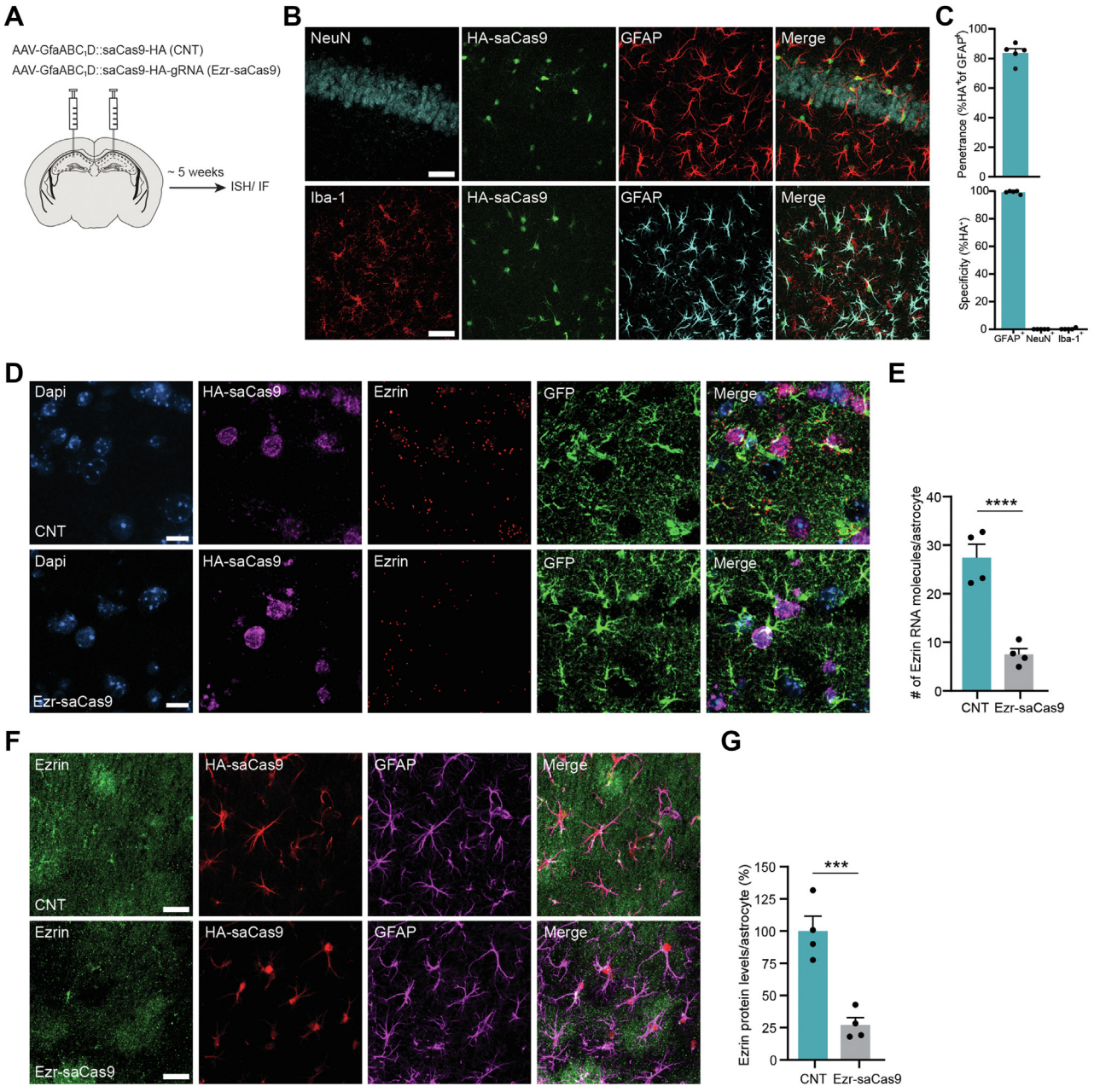

Figure 2. CRISPR/saCas9 viral approach to target *Ezr* in adult hippocampal astrocytes in vivo. **(A)** Experimental workflow: CNT and Ezr-saCas9 AAVs were microinjected bilaterally in the CA1. IF and ISH experiments were performed 5 weeks later. **(B)** Representative images of the transduction and specificity of viral vectors assessed by IF. Scale bar = 50 μm. **(C)** Quantification of penetrance (718 cells from 5 mice) and specificity (NeuN: 837 cells from 5 mice, Iba-1: 364 cells from 5 mice). **(D)** RNA scope ISH representative images for CNT and Ezr-saCas9 mice. Scale bar = 10 μm. **(E)** Quantification of the number of RNA molecules of Ezrin per astrocyte (CNT: 128 cells from 4 mice, Ezr-saCas9: 179 cells from 4 mice). Nested *t* test: $t_{305} = 23.69$, $^{****}p < .00001$. **(F)** IF representative images for CNT and Ezr-saCas9 mice. Scale bar = 30 μm. **(G)** Quantification of Ezrin protein levels per astrocyte (%) (CNT: 110 astrocytes from 4 mice, Ezr-saCas9: 102 astrocytes from 4 mice). Nested *t* test: $t_{82} = 15.09$, $^{***}p = .0001$. Data are presented as mean ± SEM. AAV, adeno-associated virus; CNT, control; CRISPR, clustered regularly interspaced short palindromic repeats; GFP, green fluorescent protein; HA, hemagglutinin tag; IF, immunofluorescence; ISH, in situ hybridization.

hippocampus. To this end, we made use of a Napa-a viral vector (42) to visualize astrocyte territories in the CA1 region of the hippocampus in the presence and absence of CRISPR (clustered regularly interspaced short palindromic repeats)/saCas9-mediated deletion of *Ezr*. We found that Ezr-saCas9 mice had smaller astrocyte territories compared with control mice (Figure 3A–C). To determine whether this smaller territory in Ezr-saCas9 mice was accompanied by shorter astrocyte leaflets, we measured their proximity to synapses using the FRET-based Napa technique that captures spatial interactions

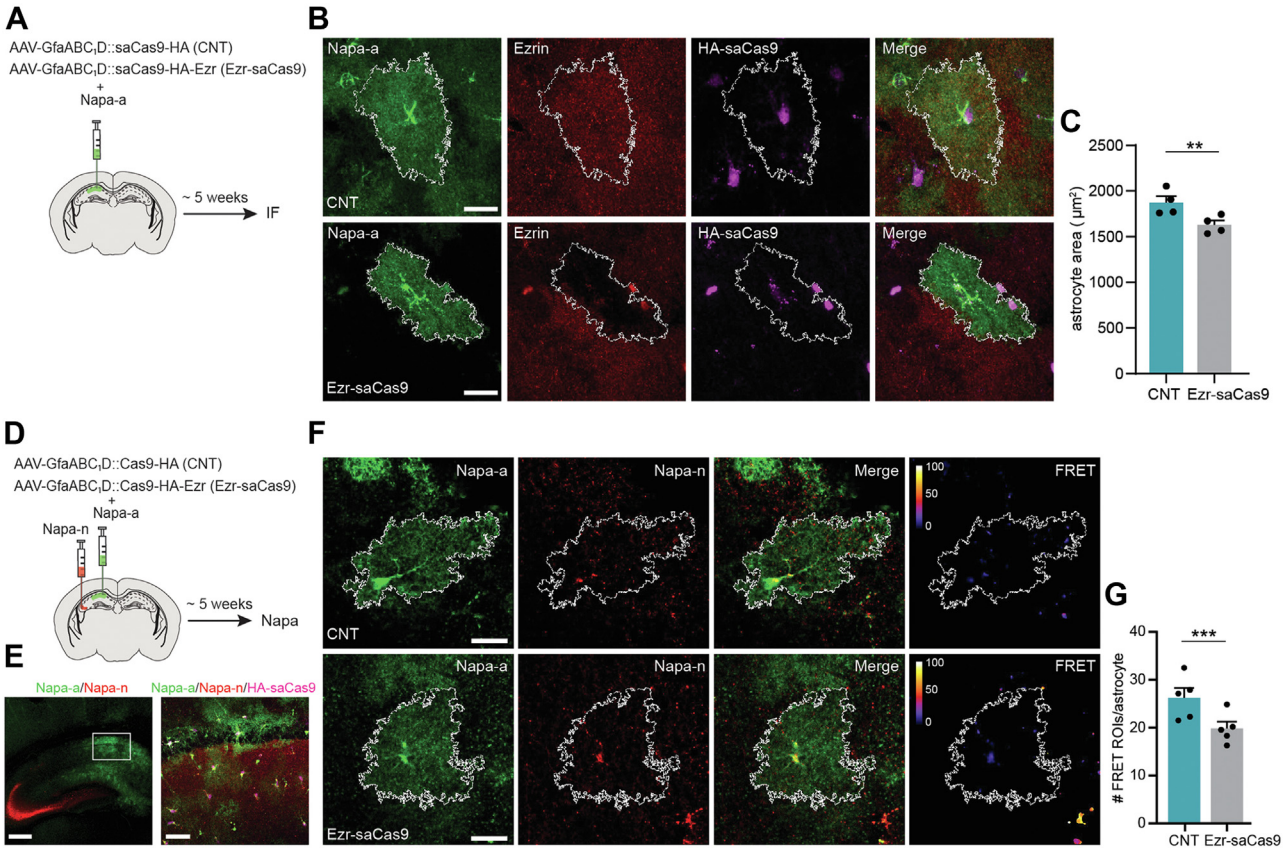

Figure 3. Deletion of *Ezr* in mature astrocytes reduces morphological complexity and neuron-astrocyte interaction. **(A)** Experimental workflow to assess astrocyte morphology. **(B)** Representative images of the astrocyte domain for CNT and Ezr-saCas9 mice. Astrocyte territory is outlined in white. Scale bar = 20 µm. **(C)** Quantification of the astrocyte territory area (μm^2) (CNT: 108 astrocytes from 4 mice, Ezr-saCas9: 109 astrocytes from 4 mice). Nested *t* test: t_{191} = 3.78, $^{**}p$ = .002. **(D)** Experimental workflow to assess the proximity of CA1 astrocyte leaflets to Schaffer collateral inputs using Napa. **(E)** (Left) Representative expression of Napa-n (red) and Napa-a (green) in the CA3 and CA1, respectively. Scale bar = 500 µm. (Right) Representative image of CA1 astrocytes expressing Napa-a (green) together with HA-saCas9 (magenta) and presynaptic puncta from CA3 projecting neurons (red). Scale bar = 50 µm. **(F)** Representative images of CA1 astrocytes from CNT and Ezr-saCas9 mice expressing Napa-a (green) in proximity to projections from CA3 neurons expressing Napa-n (red). The FRET ROIs are shown on a color scale that reflects FRET efficiency. Scale bar = 20 µm. **(G)** Quantification of the number of FRET signals (ROIs) per CA1 astrocyte (CNT: 101 astrocytes from 5 mice, Ezr-saCas9: 141 astrocytes from 5 mice). Nested *t* test: t_{63} = 3.97, $^{***}p$ = .0002. Data are presented as mean ± SEM. CNT, control; FRET, Föster resonance energy transfer; IF, immunofluorescence; ROI, region of interest.

within an approximately 10-nm range between astrocyte processes and synapses in acute brain slices (42). Astrocytic membranes in the CA1 stratum radiatum were labeled with the FRET donor GFP (green fluorescent protein) (Napa-a), and Schaffer collateral presynaptic terminals were labeled with the FRET acceptor mCherry (Napa-n) to allow detection of FRET signals at the synaptic scale. We prepared acute hippocampal slices 4 to 5 weeks after viral injection and, using confocal imaging to detect FRET signals in the CA1 (Figure 3D, E), we found that the number of synapses contacted by an astrocyte was significantly reduced in Ezr-saCas9 mice compared with control mice (Figure 3F, G). Importantly, this reduction in FRET was not due to differential expression of Napa-a or Napa-n across groups (Figure S3).

Ezrin Is Required for Close Proximity of Astrocyte Leaflets to the Synaptic Cleft

Next we used EM to closely evaluate the ultrastructure of synapses in the absence of astrocytic ezrin. Ezr-saCas9 and control virus were injected in the CA1 together with AAV-GfaABC$_1$D-GFP to visualize the injection site and confirm sufficient viral expression in samples that were subject to EM analysis (Figure 4A; Figure S4A). Our manipulation did not change the number of synapses contacted by an astrocyte (Figure 4C); instead, we found that the leaflet tip, which is in direct opposition to the synaptic cleft, was shorter in Ezr-saCas9 mice (Figure 4D, E). Consequently, we observed an increased distance between the astrocyte leaflet tip and the synaptic cleft in Ezr-saCas9 mice (Figure 4F, G). It should be noted that our manipulation slightly reduced astrocytic contact with the presynaptic button (Figure S4B), whereas it did not change contact of astrocytes with postsynaptic spines (Figure S4C) or affect the perimeter of the pre- and postsynaptic elements (Figure S4D, E). Notably, the reduction of astrocytic synaptic coverage following deletion of *Ezr* highly resembles the physiological reduction of astrocytic synaptic coverage observed at 5 days after fear conditioning, i.e., increased shorter leaflet tips and reduced longer

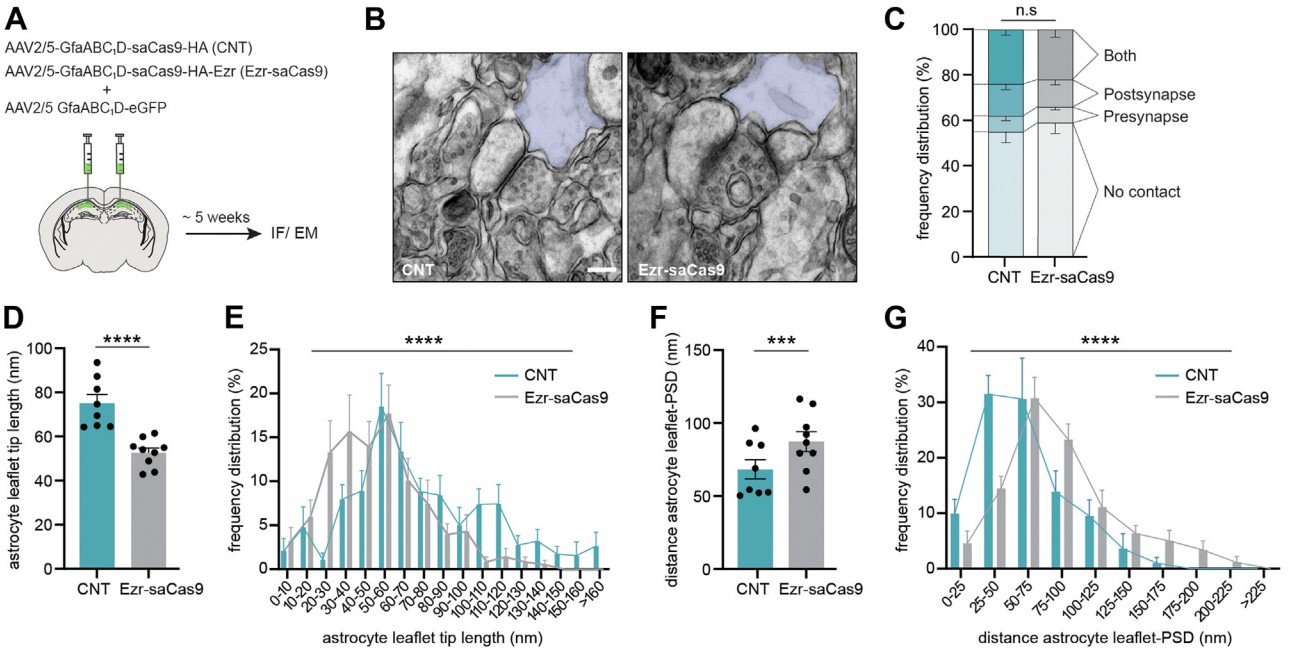

Figure 4. Depletion of ezrin levels in hippocampal astrocytes increases the distance between astrocytic leaflets and the synaptic cleft. **(A)** Experimental workflow. CNT and Ezr-Cas9 AAVs were injected in a cocktail with AAV-GfaABC$_1$D-eGFP to visualize the injection site prior to EM analysis. **(B)** Representative images of synapse structure from CNT and Ezr-saCas9 mice. In light purple, an astrocyte leaflet contacting an excitatory synapse is depicted. Scale bar = 200 nm. **(C)** Frequency distributions for the different types of astrocyte leaflet-synapse contact: synapse without an astrocyte contact (no contact), astrocyte leaflet contacts only the presynaptic button (presynapse), astrocyte leaflet contacts only the postsynapse spine (postsynapse), and astrocyte leaflet contacts both synaptic elements (both): $\chi^2_{4,258} = -0.38$, $p = .98$. **(D)** Quantification of astrocyte leaflet tip length from CNT and Ezr-saCas9 mice (CNT: 181 astrocytes from 8 mice, Ezr-saCas9: 179 astrocytes from 9 mice). Nested *t* test: $t_{352} = 7.17$, $^{****}p < .0001$. **(E)** Frequency distribution plot from data presented in **(D)**. Note that Ezr-saCas9 mice show a clear shift toward a smaller astrocyte leaflet tip. Mann-Whitney *U* test $^{****}p < .0001$. **(F)** Quantification of the distance between the astrocyte leaflet tip and the PSD from CNT and Ezr-saCas9 mice (CNT: 176 astrocytes from 8 mice, Ezr-saCas9: 173 astrocytes from 9 mice). Nested *t* test: $t_{161} = 5.1$, $^{***}p = .0001$. **(G)** Frequency distribution plot from data presented in panel **(F)**. Note that Ezr-saCas9 mice show a shift toward larger distances. Mann-Whitney *U* test $^{****}p < .0001$. Data are presented as mean ± SEM. AAV, adeno-associated virus; CNT, control; EM, electron microscopy; IF, immunofluorescence; n.s., not significant; PSD, postsynaptic density.

leaflet-postsynaptic density distances (Figure S4F, G). Taken together, these data show that the depletion of ezrin in astrocytes is an adequate mimic of the leaflet retraction that occurs after fear conditioning.

Reduced Astrocyte Contact Decreases Synaptic Glutamate Levels

To examine whether Ezr-saCas9-mediated manipulation of astrocyte leaflet structure has consequences for synaptic function, we analyzed excitatory synaptic transmission 5 weeks after virus injection in CA1 (Figure 5A). Whole-cell patch-clamp recordings from hippocampal pyramidal neurons revealed no change in spontaneous excitatory postsynaptic current (sEPSC) amplitude and frequency, suggesting that basal synaptic transmission was unaffected in Ezr-saCas9 mice (Figure 5B–D). Next we measured evoked AMPA receptor (AMPAR)–mediated EPSCs and synaptic glutamate levels in Ezr-saCas9 mice. For this, CA3-CA1 Schaffer collaterals were stimulated with or without gamma-D-glutamylglycine (γ-DGG), a low-affinity competitive antagonist of AMPARs, at a non-saturating concentration (1 mM) (43). At this concentration, the effectiveness of the drug depends on synaptic glutamate levels. Evoked EPSC amplitude and decay kinetics were not changed prior to drug application (Figure S5A–C). However, we found that γ-DGG inhibition of evoked AMPAR EPSCs was more pronounced in pyramidal cells from Ezr-saCas9 mice than from control mice (Figure 5E–H). Together, this shows that basal strength of synaptic transmission was unaffected in Ezr-saCas9 mice, but that evoked synaptic glutamate levels were reduced in Ezr-saCas9 mice compared with control mice. While this reduction was apparently not sufficient to affect spontaneous or evoked AMPAR EPSC amplitude, it altered the competition between γ-DGG and glutamate. To determine whether a reduction in presynaptic release probability (26) underlies the observed γ-DGG effect in Ezr-saCas9 mice, we examined the paired-pulse ratio and found no significant differences between Ezr-saCas9 mice and control mice (Figure 5I, J). Thus, we showed that Ezr-saCas9 mice have reduced synaptic glutamate levels after stimulation of glutamatergic terminals, which is likely not due to a presynaptic release defect.

Increased Glutamate Spillover and NMDA Receptor Activation Upon Shortening of Astrocyte Leaflets

Next, the temporal dynamics of extrasynaptic glutamate were investigated. For this, the glutamate sensor iGluSnFR (44) was

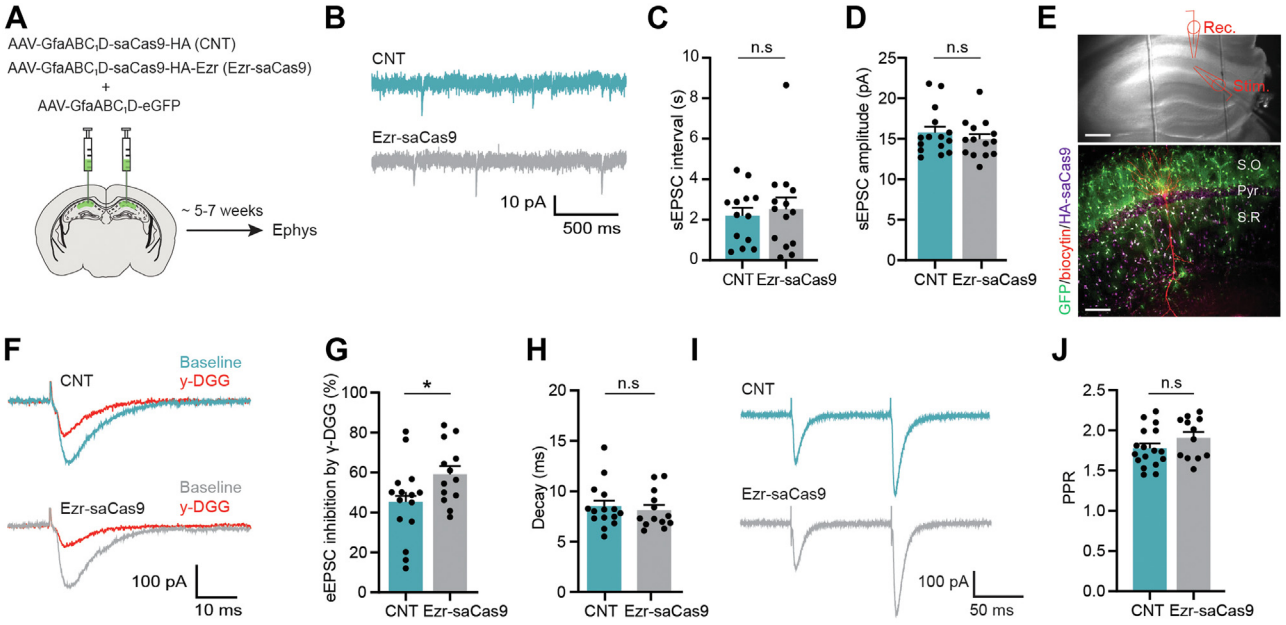

Figure 5. Reduced astroglial contact due to loss of ezrin does not affect basal synaptic transmission, but it decreases synaptic glutamate levels. **(A)** Experimental workflow. Mice were injected with CNT or Ezr-saCas9 AAVs in a cocktail with AAV-GfaABC$_1$D-eGFP for visualization purposes. Whole-cell recordings were performed 5 to 7 weeks later. **(B)** Representative traces of spontaneous AMPA receptor EPSCs from pyramidal neurons from CNT and Ezr-saCas9 mice. **(C, D)** Quantification of **(C)** interval and **(D)** amplitude of sEPSCs (CNT: 13–14 cells from 7 mice, Ezr-saCas9: 14–15 cells from 7 mice). Unpaired *t* test: (interval) $t_{25} = 0.45$, $p = .65$; (amplitude) $t_{27} = 0.81$, $p = .42$; n.s. **(E)** (Top) Representative image of the dorsal hippocampus with an adjacently placed glass pipette (rec.). The stimulation glass pipette was placed in the stratum radiatum. Scale bar = 200 μm. (Bottom) Representative image of a patched neuron filled with biocytin (red) surrounded by astrocytes expressing GFP and HA-saCas9. Scale bar = 100 μm. **(F)** Representative traces of evoked AMPA receptor EPSCs from pyramidal neurons from CNT and Ezr-saCas9 mice with and without γ-DGG (1 mM). **(G, H)** Quantification of the **(G)** percentage of evoked EPSC amplitude inhibited by γ-DGG and **(H)** decay kinetics in presence of γ-DGG (CNT: 15 cells from 6 mice, Ezr-saCas9: 13 cells from 6 mice). Unpaired *t* test: (amplitude) $t_{26} = 2.087$, $^*p = .04$; (decay) $t_{26} = 0.46$, $p = .64$; n.s. **(I)** Representative traces of PPR from CNT and Ezr-saCas9 mice. **(J)** Quantification of PPR from CNT and Ezr-saCas9 mice (CNT: 17 cells from 7 mice, Ezr-saCas9: 12 cells from 7 mice). Unpaired *t* test: $t_{27} = 1.38$, $p = .17$. Data are presented as mean ± SEM. AAV, adeno-associated virus; CNT, control; Ephys, electrophysiology; γ-DGG, gamma-D-glutamylglycine; sEPSC, spontaneous excitatory postsynaptic current; GFP, green fluorescent protein; n.s., not significant; PPR, paired-pulse ratio; Rec., recording; Stim., stimulation.

expressed in CA1 astrocytes together with either Ezr-saCas9 or control virus (Figure 6A). Two-photon imaging of iGluSnFR signals allowed us to study the time course of extrasynaptic glutamate following synaptic stimulation. Synaptic activity was evoked by focal electrical stimulation (10 pulses at 50 Hz) in the CA1 (Figure 6B). We did not observe significant changes in the magnitude of iGluSnFR signal between groups (Figure S6A, B). To examine temporal dynamics of glutamate levels, we fitted the decay of the averaged evoked glutamate transients (6 sweeps) with a single exponential and found that the glutamate transients in Ezr-saCas9 mice displayed an increased decay time following trains of 50 Hz stimulation (Figure 6C–E). The decay of the iGluSnFR transients was not influenced by the amplitude of the response (Figure S6C, D). These data suggest increased dwelling of glutamate in the extrasynaptic space after depletion of ezrin in astrocytes, which is in line with the observed decrease in astroglial coverage of excitatory synapses in Ezr-saCas9 mice.

Because astrocyte leaflets contain the high-affinity glutamate transporter GLT-1, we next tested whether the lack of ezrin might slow glutamate clearance. We found that partial blockade of glutamate transporters with threo-beta-benzyloxyaspartate (DL-TBOA) (10 μM) similarly significantly increased the decay kinetics of glutamate transients in both groups (Figure S6E, F). These data suggest that even though astrocyte leaflets are farther away from the synaptic cleft in Ezr-saCas9 mice, the uptake of glutamate remains unchanged.

Perisynaptic glutamate has been shown to increase the activation of extrasynaptic NMDA receptors (45). Therefore, we stimulated CA1 pyramidal neurons with incremental short bursts (1-2-4-8 stimuli) of high-frequency stimulation (100 Hz) to increase glutamate spillover (46) and measured NMDA receptor (NMDAR)–mediated EPSCs (Figure 6A). Ezr-saCas9 mice showed a remarkable increase in NMDAR-mediated evoked EPSCs with increased stimulation frequency, resulting from a larger amplitude of events as well as slower decay (Figure 6F–H; Figure S7A–C). These results are consistent with the interpretation that reduced astrocyte leaflet-synapse interaction leads to enhanced synaptic cooperation (via activation of extrasynaptic NMDARs and/or NMDARs in neighboring synapses) (33,47). Next we determined whether enhanced NMDAR activation was an endogenous process occurring during fear memory consolidation as a result of astrocyte leaflet retraction (Figure 1). We found that mice that underwent CFC showed an increase in NMDAR-mediated evoked EPSCs (Figure 6I, J; Figure S7D–F), similar to the effects observed in Ezr-saCas9 mice. Taken together, these

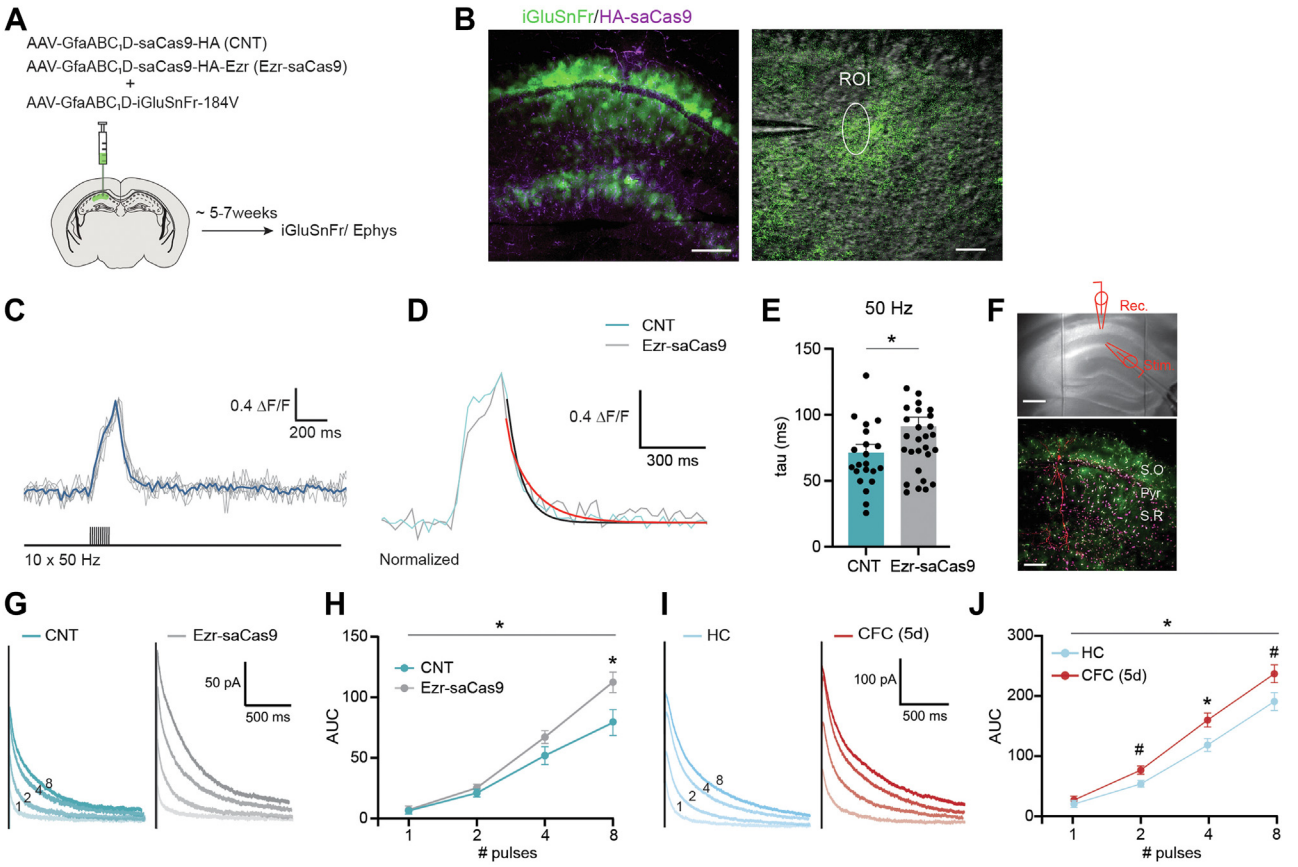

Figure 6. Decreased astroglial synaptic contact boosts glutamate spillover and NMDA receptor activation. **(A)** Experimental workflow. Mice were injected with CNT and Ezr-saCas9 AAVs in a cocktail with AAV-GfaABC$_1$D-iGluSnFr. Five weeks later, glutamate and electrophysiological measurements were performed. **(B)** (Left) Representative images of CA1 astrocytes expressing AAV-GfaABC$_1$D::iGluSnFR and AAV-GfaABC$_1$D::Cas9-HA-Ezr. Scale bar = 200 μm. (Right) Stimulation glass pipette was placed adjacently to an astrocyte expressing iGluSnFR, and transients were measured and quantified from the ROI. Scale bar = 20 μm. **(C, D)** Upon synaptic stimulation (10 × 50 Hz), a robust increase in iGluSnFR signal was detected. **(C)** Thick blue line represents the average of 6 responses. **(D)** Thick black (CNT) and red (Ezr-saCas9) lines represent the single-exponential fit of the decay. **(E)** Quantification of the decay kinetics (CNT: 22 astrocytes from 7 mice, Ezr-saCas9: 31 astrocytes from 7 mice) following 50 Hz stimulation. Unpaired *t* test: $t_{51} = 2.06$, $^*p = .02$. **(F)** (Top) Representative image of the dorsal hippocampus with an adjacently placed glass pipette (rec.). The stimulation glass pipette was placed in the stratum radiatum. Scale bar = 200 μm. (Bottom) Representative image of a patched neuron filled with biocytin (red) surrounded by astrocytes expressing AAV-GfaABC$_1$D::GFP and AAV-GfaABC$_1$D::saCas9-HA-Ezr. Scale bar = 100 μm. **(G)** Representative traces of the NMDA receptor EPSCs upon incremental short burst stimulation (1,2,4,8) for CNT and Ezr-saCas9 mice. **(H)** Quantification of the AUC (CNT: 17 cells from 7 mice, Ezr-saCas9: 27 cells from 9 mice). Repeated-measures two-way ANOVA, interaction effect pulses × genotype; $F_{1.23,15.17} = 6.67$, $^*p = .01$. Post hoc Bonferroni test control vs. Ezr-saCas9: 1 pulse $p = .97$, 2 pulses $p = .77$, 4 pulses $p = .35$, 8 pulses $^*p = .03$. **(I)** Representative traces of the NMDA receptor EPSCs upon incremental short burst stimulation (1,2,4,8) for HC and fear-conditioned mice. **(J)** Quantification of the AUC (HC: 21 cells from 6 mice, CFC: 18 cells from 6 mice). Repeated-measures two-way ANOVA, interaction effect pulses × genotype; $F_{1.24,18.28} = 4.96$, $^*p = .03$. Post hoc Bonferroni test HC vs. CFC: 1 pulse $p = .12$, 2 pulses $p = .05$, 4 pulses $p = .04$, 8 pulses $p = .08$. Data are presented as mean ± SEM. AAV, adeno-associated virus; ANOVA, analysis of variance; AUC, area under the curve; CFC, contextual fear conditioning; CNT, control; Ephys, electrophysiology; EPSCs, excitatory postsynaptic currents; HC, home cage; Rec., recording; ROI, region of interest; Stim., stimulation.

results showed that increased activation of hippocampal NMDARs upon CFC can be recapitulated by saCas9-induced astrocyte leaflet retraction through depletion of astrocytic ezrin.

Shortening of Astrocyte Leaflets Enhances Recent Contextual Fear Memory Retrieval and Increases Neuronal Activity

Next, mice were fear conditioned 5 weeks after viral delivery, and memory expression was measured at recent and remote time points after learning. Ezr-saCas9 mice exhibited enhanced fear expression when compared with control mice 5 days after CFC (Figure 7B), a phenotype that was replicated using a second sgRNA that targets a different region of the *Ezr* gene (Figure S8). No change in freezing levels were detected 28 days after CFC (Figure S9A). Furthermore, no differences were found between control mice and Ezr-saCas9 mice in the open field, indicating that the observed phenotype was not driven by anxiety or locomotor deficits (Figure S9B–D). Furthermore, no effect on freezing levels was detected in an independent cohort of mice that was trained in the conditioning box but placed in a novel context 5 days later (Figure 7A, C), demonstrating that the enhanced fear memory was context specific and time dependent.

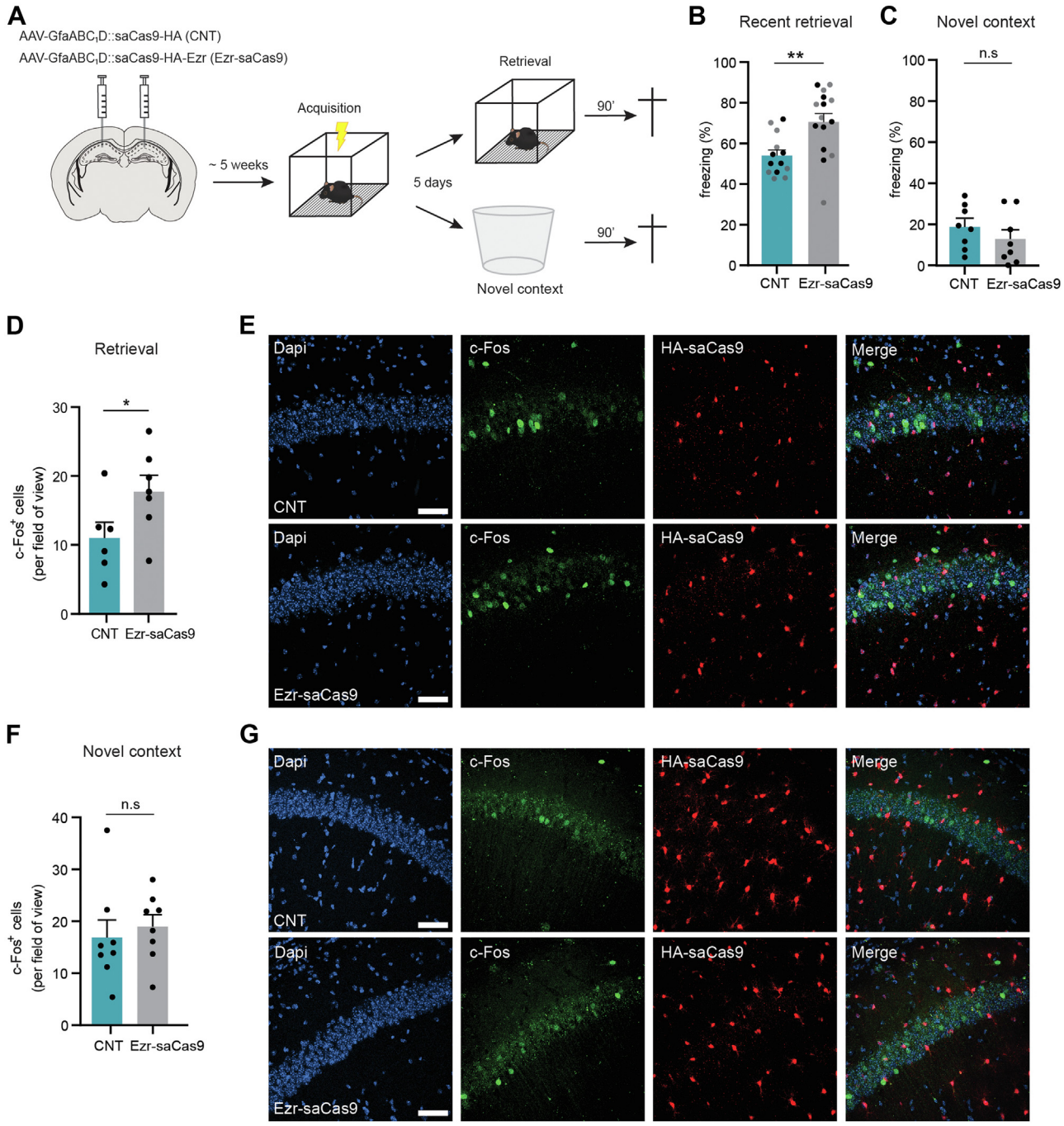

Figure 7. Enhanced expression of recent contextual fear memory and c-Fos$^+$ cells in Ezr-saCas9 mice. **(A)** Experimental workflow. Mice were injected with CNT and Ezr-saCas9 AAVs in the CA1, and 5 weeks later, fear conditioning or novel context was performed. Mice were sacrificed 90 minutes after retrieval. **(B)** Freezing levels during retrieval. Data pooled from 2 independent cohorts of mice color-coded in black and gray (CNT: 13 mice and Ezr-saCas9: 15 mice). Unpaired *t* test: $t_{26} = 3.16$, $^{**}p = .004$. **(C)** Freezing levels during novel context (CNT and Ezr-saCas9: 8 mice). Unpaired *t* test: $t_{14} = 0.96$, $p = .35$. **(D)** Quantification of c-Fos$^+$ cells in the CA1 pyramidal layer during recent retrieval (CNT: 8 slices per mouse from 6 mice, Ezr-saCas9: 8 slices per mouse from 7 mice). Samples correspond to the cohort of mice highlighted in black in panel **(B)**. Unpaired *t* test: $t_{11} = 2.27$, $^{*}p = .04$. **(E)** Representative examples of activated neurons (c-Fos$^+$ cells) in the CA1 during recent retrieval. **(F)** Quantification of c-Fos$^+$ cells in the CA1 pyramidal layer during novel context exposure (Control: 8 slices per mouse from 8 mice, Ezr-saCas9: 8 slices per mouse from 8 mice). Unpaired *t* test: $t_{14} = 0.52$, $p = .6$. **(G)** Representative examples of activated neurons (c-Fos$^+$ cells in the CA1 during novel context). Scale bar = 50 μm. Data are presented as mean ± SEM. AAV, adeno-associated virus; CNT, control; n.s., not significant.

Next we tested whether memory enhancement was accompanied by increased neuronal activity in a context-dependent manner. For this, we quantified the number of neurons that expressed c-Fos [an established marker for neuronal activation (48)] in CA1 of mice that underwent retrieval in the conditioning context, mice that were placed in novel context during retrieval, and naïve HC control mice. In line with the enhanced freezing levels observed, Ezr-saCas9 mice had a greater number of c-Fos$^+$ neurons after recent retrieval than control mice (Figure 7D, E). Notably, this increased neuronal activation was context and memory specific because no differences were observed between groups after retrieval in a novel context (Figure 7F, G) or in naïve HC control mice (Figure S9E, F). Together, these data demonstrate that interaction between astrocyte leaflets and synapses in the hippocampus influences recent memory retrieval and gates neuronal activation in a context-dependent manner.

DISCUSSION

Our data reveal that processing of contextual fear memory induces structural remodeling of astrocyte leaflets in the hippocampus and that the proximity of these specialized structures to the synaptic cleft determines the strength of recent memory expression. In line with the critical role of astrocyte leaflets in fear memory processing, we also showed that genetic deletion of *Ezr* enhanced glutamate spillover, NMDAR activation, and recent memory expression.

Previous studies using acute hippocampal slices have proposed that synaptic potentiation induces a robust retraction of astroglial processes from hippocampal synapses within a timeframe of 10 to 90 minutes after stimulation (33,34). We demonstrated in vivo that astrocyte leaflet retraction occurs rapidly (30 minutes) and is maintained within the first 5 days after CFC. Notably, this retraction is no longer present 4 weeks after learning. It should be noted that Mazaré *et al.* (49) reported unchanged leaflet-to-synapse distance after recent retrieval; however, an important difference from our study is that we did not include a retrieval session. In addition, hyperthin structures previously observed with EM might remain elusive with super-resolution microscopy (49–52). Our data are in line with the theory that recent memories ($<$1 week old) rely on orchestrated activity in the hippocampus (6,40) whereas remote memories ($\geq$1 month old) depend on network-wide changes involving cortical regions (53–55). Whether astrocyte leaflets also retract from inhibitory synapses during fear memory consolidation, thereby contributing to GABA (gamma-aminobutyric acid) spillover, remains to be determined. The cause and functional relevance of the increased spine size after 4 weeks of learning are unclear and are important topics for future research.

Recent studies have demonstrated a crucial role for astrocyte-neuron signaling in shaping neuronal circuits and behavior (12,13,15,16,56–60), and much of this work is based on the assumption that astrocytes' processes are located in close proximity to synapses. However, how this proximity, which we showed is dynamic (Figure 1), affects cognitive performance remains largely unexplored (25,61). We used CRISPR/saCas9 gene editing to manipulate astrocyte processes by targeting *Ezr*. It should be noted, however, that the Ezr-saCas9 vector did not lead to a complete absence of astrocytic ezrin; therefore, some of the effects caused by ezrin depletion are likely to be an underestimation. We showed that in vivo reduction of ezrin in adult hippocampal astrocytes affects astrocyte morphogenesis and increases the distance between the astrocyte leaflet and synaptic cleft. This implies that astrocytic ezrin could link membrane-bound proteins with actin filaments and may thereby be essential in the formation and motility of the fine glial processes upon specific stimuli (62). This mechanism has been suggested for other actin-binding proteins, such as cofilin-1, which regulates leaflet shrinkage through NKCC1 (Na^+, K^+, $2Cl^-$ cotransporter) activation (33), and profilin-1, which regulates leaflet outgrowth upon Ca^{2+} elevation (63). Based on previous studies performed in epithelial cells, ezrin undergoes a C-terminal phosphorylation/dephosphorylation cycle that regulates its apical membrane localization and that is necessary for microvilli formation (64,65). Therefore, it would be of particular interest to determine whether a phosphorylation/dephosphorylation cycle drives ezrin-dependent leaflets' structural plasticity upon neuronal activity and during the processing of aversive memories.

Astrocytes are intimately associated with synapses both structurally and functionally (22,34,50,66–68). Considering that our manipulation affected the spatial organization of leaflets at synapses, we examined excitatory synaptic transmission. First, we found that the lack of astrocytic ezrin had no effect on basal synaptic transmission. In line with this, reduction of astrocyte territory and astrocyte-synapse interaction by deletion of the astrocyte transcription factor NFIAA in the hippocampus had no effect on basal synaptic function (69). In fact, ezrin-dependent astrocyte leaflet-synapse interaction becomes apparent only in response to strong activation of local synapses, e.g., incremental burst stimulation that leads to NMDAR activation (Figure 6) or learning-induced synaptic activation (Figure 7). Thus, the increased NMDAR-mediated responses we observe during fear memory consolidation and in Ezr-saCas9 mice are likely a consequence of increased glutamate spillover during repetitive synaptic stimulation (70,71). This is consistent with previous findings in hippocampal acute slices, wherein long-term potentiation–induced leaflet withdrawal enhanced the activation of extrasynaptic NMDARs and facilitated NMDAR-mediated crosstalk among neighboring synapses (33). It should be noted, however, that increased glutamate spillover has been found to activate presynaptic and postsynaptic (extrasynaptic) metabotropic glutamate receptors, thereby regulating synaptic strength and neuronal excitability (72–74). Nevertheless, our observation that paired-pulse ratio is not affected in Ezr-saCas9 mice suggests that presynaptic metabotropic glutamate receptors on glutamatergic terminals are likely not involved (26). Furthermore, we showed that the increased glutamate spillover and NMDAR activation in the Ezr-saCas9 mice likely reflects an increased diffusion in the extracellular space (75) because glutamate clearance does not seem to be impaired. Taken together, our data reveal that while a decrease in synaptic coverage does not affect basal synaptic transmission, it is sufficient to boost glutamate spillover and (extra) synaptic NMDAR activation under conditions of robust neuronal activation.

Numerous studies have provided evidence that altered communication between astrocytes and neurons facilitates the development of psychiatric disorders (8,9,30,31,57,76); however, it remains poorly understood whether changes in the proximity of the astrocyte leaflet to the synapse underlie such maladaptive responses. Nonetheless, Pannasch *et al.* (61) showed that deletion of connexin 30, a gap-junction protein, causes astroglial penetration of the synaptic cleft and subsequent impairment of synaptic strength and contextual fear memory retrieval. However, leaflet insertion into the cleft has so far not been observed under physiological and/or pathological conditions or in the conditions tested in this study. Conversely, we demonstrated that when the astrocyte leaflet is farther away from the synaptic cleft, mice exhibited increased glutamate spillover and enhanced fear memory expression. Interestingly, we observed that this increased recall is time and context specific, which is in line with previous studies demonstrating the importance of the hippocampus in encoding the contextual component of recent memories (6,53). Furthermore, Ezr-saCas9 mice showed an increase in retrieval-evoked neuronal activity, suggesting that astrocytes show a tailored response to the activity of their surrounding neurons (12). Accordingly, we think that learning-induced increase in glutamate spillover, due to reduced astroglial synaptic coverage, may promote the engagement of synapses that are in close proximity and consequently enhance synaptic connectivity to strengthen memory consolidation and/or retrieval (11). Whether astrocyte leaflet retraction is a process that also occurs upon the formation and consolidation of neutral and/or positive memories is an important unanswered question.

To conclude, we discovered that fear learning induces transient retraction of astrocyte leaflets during memory formation and consolidation and experimentally determined that the proximity of astrocyte leaflets to the synaptic cleft enhances NMDAR activation and the expression of contextual fear memory. To our knowledge, this is the first study to show that a selective and physiologically relevant manipulation of the structure of astrocyte leaflets leads to enhanced contextual fear memory retrieval. Our data support the proposition that the proximity of astrocyte leaflets to synapses in the adult brain has an important role in shaping the plasticity mechanisms that underlie the processing of aversive events.

ACKNOWLEDGMENTS AND DISCLOSURES

AB-S received funding from the EU-FP7-PEOPLE program (CognitionNET; Grant No. 607509). MSJK received funding from ZonMW Memorable (Grant No. 7330508160).

AB-S performed stereotaxic surgeries, histology, confocal imaging, Napa, 2-photon glutamate imaging, and all behavioral experiments. MSJK and AM performed electron microscopy experiments. TSH performed all electrophysiological experiments. BK cosupervised the Napa experiments. RM cosupervised electrophysiological and 2-photon experiments. AN built the 2-photon microscope. MCvdO critically revised the manuscript. MHGV, AB-S, and ABS conceived the project. MHGV and ABS supervised all aspects of the project and secured funding. AB-S and MHGV wrote the manuscript with input from all the other authors.

We thank Yvonne Gouwenberg and Robbert Zalm (Vrije Universiteit Amsterdam, Amsterdam, the Netherlands) for AAV vector construct preparation, Rolinka van der Loo and Joke Wortel (Vrije Universiteit Amsterdam, Amsterdam, the Netherlands) for helping with animal perfusions, J. Christopher Octeau for technical support during Napa experiments, and Priyanka Rao-Ruiz (Vrije Universiteit Amsterdam, Amsterdam, the Netherlands) for critical revision of the manuscript.

A previous version of this article was published as a preprint on bioRxiv: http://doi.org/10.1101/2022.01.30.478393/.

The authors report no biomedical financial interests or potential conflicts of interest.

ARTICLE INFORMATION

From the Department of Molecular and Cellular Neuroscience, Center for Neurogenomics and Cognitive Research, Amsterdam Neuroscience, Vrije Universiteit Amsterdam, Amsterdam, the Netherlands (AB-S, MSJK, AM, MCvdO, ABS, MHGV); Department of Integrative Neurophysiology, Center for Neurogenomics and Cognitive Research, Amsterdam Neuroscience, Vrije Universiteit Amsterdam, Amsterdam, the Netherlands (TSH, AN, HDM, RM); Department of Child Neurology, Emma Children's Hospital, Amsterdam University Medical Centers, Amsterdam Neuroscience, Vrije Universiteit Amsterdam, Amsterdam, the Netherlands (RM); Department of Physiology, David Geffen School of Medicine, University of California, Los Angeles, Los Angeles, California (BSK); and the Department of Neurobiology, David Geffen School of Medicine, University of California, Los Angeles, Los Angeles, California (BSK).

Address correspondence to Mark H.G. Verheijen, Ph.D., at mark.verheijen@vu.nl.

Received Apr 22, 2022; revised Oct 7, 2022; accepted Oct 20, 2022.

Supplementary material cited in this article is available online at https://doi.org/10.1016/j.biopsych.2022.10.013.

REFERENCES

1. Izquierdo I, Furini CRG, Myskiw JC (2016): Fear memory. Physiol Rev 96:695–750.
2. Knight DC, Smith CN, Cheng DT, Stein EA, Helmstetter FJ (2004): Amygdala and hippocampal activity during acquisition and extinction of human fear conditioning. Cogn Affect Behav Neurosci 4:317–325.
3. Goosens KA (2011): Hippocampal regulation of aversive memories. Curr Opin Neurobiol 21:460–466.
4. Duvarci S, Pare D (2014): Amygdala microcircuits controlling learned fear. Neuron 82:966–980.
5. Rao-Ruiz P, Couey JJ, Marcelo IM, Bouwkamp CG, Slump DE, Matos MR, *et al.* (2019): Engram-specific transcriptome profiling of contextual memory consolidation. Nat Commun 10:2232.
6. Liu X, Ramirez S, Pang PT, Puryear CB, Govindarajan A, Deisseroth K, Tonegawa S (2012): Optogenetic stimulation of a hippocampal engram activates fear memory recall. Nature 484:381–385.
7. Tayler KK, Tanaka KZ, Reijmers LG, Wiltgen BJ (2013): Reactivation of neural ensembles during the retrieval of recent and remote memory. Curr Biol 23:99–106.
8. Leuner B, Falduto J, Shors TJ (2003): Associative memory formation increases the observation of dendritic spines in the hippocampus. J Neurosci 23:659–665.
9. Geinisman Y, Berry RW, Disterhoft JF, Power JM, Van der Zee EA (2001): Associative learning elicits the formation of multiple-synapse boutons. J Neurosci 21:5568–5573.
10. Rao-Ruiz P, Visser E, Mitrić M, Smit AB, van den Oever MC (2021): A synaptic framework for the persistence of memory engrams. Front Synaptic Neurosci 13:661476.
11. Govindarajan A, Kelleher RJ, Tonegawa S (2006): A clustered plasticity model of long-term memory engrams. Nat Rev Neurosci 7:575–583.
12. Adamsky A, Kol A, Kreisel T, Doron A, Ozeri-Engelhard N, Melcer T, *et al.* (2018): Astrocytic activation generates de novo neuronal potentiation and memory enhancement. Cell 174:59–71.e14.
13. Kol A, Adamsky A, Groysman M, Kreisel T, London M, Goshen I (2020): Astrocytes contribute to remote memory formation by modulating hippocampal–cortical communication during learning. Nat Neurosci 23:1229–1239.
14. Li Y, Li L, Wu J, Zhu Z, Feng X, Qin L, *et al.* (2020): Activation of astrocytes in hippocampus decreases fear memory through adenosine A1 receptors. eLife 9:e57155.

15. Suzuki A, Stern SA, Bozdagi O, Huntley GW, Walker RH, Magistretti PJ, Alberini CM (2011): Astrocyte-neuron lactate transport is required for long-term memory formation. Cell 144:810–823.
16. Gao V, Suzuki A, Magistretti PJ, Lengacher S, Pollonini G, Steinman MQ, Alberini CM (2016): Astrocytic β_2-adrenergic receptors mediate hippocampal long-term memory consolidation. Proc Natl Acad Sci U S A 113:8526–8531.
17. Khakh BS, Sofroniew MV (2015): Diversity of astrocyte functions and phenotypes in neural circuits. Nat Neurosci 18:942–952.
18. Araque A, Carmignoto G, Haydon PG, Oliet SHR, Robitaille R, Volterra A (2014): Gliotransmitters travel in time and space. Neuron 81:728–739.
19. Semyanov A, Verkhratsky A (2021): Astrocytic processes: From tripartite synapses to the active milieu. Trends Neurosci 44:781–792.
20. Ghézali G, Dallérac G, Rouach N (2016): Perisynaptic astroglial processes: Dynamic processors of neuronal information. Brain Struct Funct 221:2427–2442.
21. Bazargani N, Attwell D (2016): Astrocyte calcium signaling: The third wave. Nat Neurosci 19:182–189.
22. Araque A, Parpura V, Sanzgiri RP, Haydon PG (1999): Tripartite synapses: Glia, the unacknowledged partner. Trends Neurosci 22:208–215.
23. Derouiche A, Frotscher M (2001): Peripheral astrocyte processes: Monitoring by selective immunostaining for the actin-binding ERM proteins. Glia 36:330–341.
24. Lavialle M, Aumann G, Anlauf E, Pröls F, Arpin M, Derouiche A (2011): Structural plasticity of perisynaptic astrocyte processes involves ezrin and metabotropic glutamate receptors. Proc Natl Acad Sci U S A 108:12915–12919.
25. Zhou B, Chen L, Liao P, Huang L, Chen Z, Liao D, *et al.* (2019): Astroglial dysfunctions drive aberrant synaptogenesis and social behavioral deficits in mice with neonatal exposure to lengthy general anesthesia. PLoS Biol 17:e3000086.
26. Oliet SHR, Piet R, Poulain DA (2001): Control of glutamate clearance and synaptic efficacy by glial coverage of neurons. Science 292:923–926.
27. Panatier A, Oliet SHR (2006): Neuron–glia interactions in the hypothalamus. Neuron Glia Biol 2:51–58.
28. Becquet D, Girardet C, Guillaumond F, François-Bellan AM, Bosler O (2008): Ultrastructural plasticity in the rat suprachiasmatic nucleus. Possible involvement in clock entrainment. Glia 56:294–305.
29. Scofield MD, Li H, Siemsen BM, Healey KL, Tran PK, Woronoff N, *et al.* (2016): Cocaine self-administration and extinction leads to reduced glial fibrillary acidic protein expression and morphometric features of astrocytes in the nucleus accumbens core. Biol Psychiatry 80:207–215.
30. Siemsen BM, Reichel CM, Leong KC, Garcia-Keller C, Gipson CD, Spencer S, *et al.* (2019): Effects of methamphetamine self-administration and extinction on astrocyte structure and function in the nucleus accumbens core. Neuroscience 406:528–541.
31. Kruyer A, Scofield MD, Wood D, Reissner KJ, Kalivas PW (2019): Heroin cue–evoked astrocytic structural plasticity at nucleus accumbens synapses inhibits heroin seeking. Biol Psychiatry 86:811–819.
32. Ostroff LE, Manzur MK, Cain CK, Ledoux JE (2014): Synapses lacking astrocyte appear in the amygdala during consolidation of Pavlovian threat conditioning. J Comp Neurol 522:2152–2163.
33. Henneberger C, Bard L, Panatier A, Reynolds JP, Kopach O, Medvedev NI, *et al.* (2020): LTP induction boosts glutamate spillover by driving withdrawal of perisynaptic astroglia. Neuron 108:919–936.e11.
34. Perez-Alvarez A, Navarrete M, Covelo A, Martin ED, Araque A (2014): Structural and functional plasticity of astrocyte processes and dendritic spine interactions. J Neurosci 34:12738–12744.
35. Bernardinelli Y, Randall J, Janett E, Nikonenko I, König S, Jones EV, *et al.* (2014): Activity-dependent structural plasticity of perisynaptic astrocytic domains promotes excitatory synapse stability. Curr Biol 24:1679–1688.
36. Lushnikova I, Skibo G, Muller D, Nikonenko I (2009): Synaptic potentiation induces increased glial coverage of excitatory synapses in CA1 hippocampus. Hippocampus 19:753–762.
37. Wenzel J, Lammert G, Meyer U, Krug M (1991): The influence of long-term potentiation on the spatial relationship between astrocyte processes and potentiated synapses in the dentate gyrus neuropil of rat brain. Brain Res 560:122–131.
38. Badia-Soteras A, Octeau JC, Verheijen MHG, Khakh BS (2020): Assessing neuron–astrocyte spatial interactions using the neuron–astrocyte proximity assay. Curr Protoc Neurosci 91:e91.
39. Herde MK, Bohmbach K, Domingos C, Vana N, Komorowska-Müller JA, Passlick S, *et al.* (2020): Local efficacy of glutamate uptake decreases with synapse size. Cell Rep 32:108182.
40. Denny CA, Kheirbek MA, Alba EL, Tanaka KF, Brachman RA, Laughman KB, *et al.* (2014): Hippocampal memory traces are differentially modulated by experience, time, and adult neurogenesis. Neuron 83:189–201.
41. Ortinski PI, Dong J, Mungenast A, Yue C, Takano H, Watson DJ, *et al.* (2010): Selective induction of astrocytic gliosis generates deficits in neuronal inhibition. Nat Neurosci 13:584–591.
42. Octeau JC, Chai H, Jiang R, Bonanno SL, Martin KC, Khakh BS (2018): An optical neuron-astrocyte proximity assay at synaptic distance scales. Neuron 98:49–66.e9.
43. Liu G, Choi S, Tsien RW (1999): Variability of neurotransmitter concentration and nonsaturation of postsynaptic AMPA receptors at synapses in hippocampal cultures and slices. Neuron 22:395–409.
44. Marvin JS, Borghuis BG, Tian L, Cichon J, Harnett MT, Akerboom J, *et al.* (2013): An optimized fluorescent probe for visualizing glutamate neurotransmission. Nat Methods 10:162–170.
45. Kullmann DM, Asztely F (1998): Extrasynaptic glutamate spillover in the hippocampus: Evidence and implications. Trends Neurosci 21:8–14.
46. Lozovaya NA, Grebenyuk SE, TSh Tsintsadze, Feng B, Monaghan DT, Krishtal OA (2004): Extrasynaptic NR2B and NR2D subunits of NMDA receptors shape 'superslow' afterburst EPSC in rat hippocampus. J Physiol 558:451–463.
47. Arnth-Jensen N, Jabaudon D, Scanziani M (2002): Cooperation between independent hippocampal synapses is controlled by glutamate uptake. Nat Neurosci 5:325–331.
48. Cruz FC, Javier Rubio F, Hope BT (2015): Using c-fos to study neuronal ensembles in corticostriatal circuitry of addiction. Brain Res 1628:157–173.
49. Mazaré N, Oudart M, Moulard J, Cheung G, Tortuyaux R, Mailly P, *et al.* (2020): Local translation in perisynaptic astrocytic processes is specific and changes after fear conditioning. Cell Rep 32:108076.
50. Arizono M, Inavalli VVGK, Panatier A, Pfeiffer T, Angibaud J, Levet F, *et al.* (2020): Structural basis of astrocytic Ca2+ signals at tripartite synapses. Nat Commun 11:1906.
51. Vicidomini G, Bianchini P, Diaspro A (2018): STED super-resolved microscopy. Nat Methods 15:173–182.
52. Heller JP, Rusakov DA (2017): The nanoworld of the tripartite synapse: Insights from super-resolution microscopy. Front Cell Neurosci 11:374.
53. Frankland PW, Bontempi B (2005): The organization of recent and remote memories. Nat Rev Neurosci 6:119–130.
54. Matos MR, Visser E, Kramvis I, van der Loo RJ, Gebuis T, Zalm R, *et al.* (2019): Memory strength gates the involvement of a CREB-dependent cortical fear engram in remote memory. Nat Commun 10:2315.
55. Kitamura T, Ogawa SK, Roy DS, Okuyama T, Morrissey MD, Smith LM, *et al.* (2017): Engrams and circuits crucial for systems consolidation of a memory. Science 356:73–78.
56. Martin-Fernandez M, Jamison S, Robin LM, Zhao Z, Martin ED, Aguilar J, *et al.* (2017): Synapse-specific astrocyte gating of amygdala-related behavior. Nat Neurosci 20:1540–1548.
57. Nagai J, Rajbhandari AK, Gangwani MR, Hachisuka A, Coppola G, Masmanidis SC, *et al.* (2019): Hyperactivity with disrupted attention by activation of an astrocyte synaptogenic cue. Cell 177:1280–1292.e20.
58. Papouin T, Dunphy JM, Tolman M, Dineley KT, Haydon PG (2017): Septal cholinergic neuromodulation tunes the astrocyte-dependent

gating of hippocampal NMDA receptors to wakefulness. Neuron 94:840–854.e7.
59. Robin LM, Oliveira da Cruz JF, Langlais VC, Martin-Fernandez M, Metna-Laurent M, Busquets-Garcia A, *et al.* (2018): Astroglial CB1 receptors determine synaptic D-serine availability to enable recognition memory. Neuron 98:935–944.e5.
60. Mederos S, Sánchez-Puelles C, Esparza J, Valero M, Ponomarenko A, Perea G (2021): GABAergic signaling to astrocytes in the prefrontal cortex sustains goal-directed behaviors. Nat Neurosci 24:82–92.
61. Pannasch U, Freche D, Dallérac G, Ghézali G, Escartin C, Ezan P, *et al.* (2014): Connexin 30 sets synaptic strength by controlling astroglial synapse invasion. Nat Neurosci 17:549–558.
62. Derouiche A, Geiger KD (2019): Perspectives for Ezrin and radixin in astrocytes: Kinases, functions and pathology. Int J Mol Sci 20:3776.
63. Molotkov D, Zobova S, Arcas JM, Khiroug L (2013): Calcium-induced outgrowth of astrocytic peripheral processes requires actin binding by Profilin-1. Cell Calcium 53:338–348.
64. Viswanatha R, Ohouo PY, Smolka MB, Bretscher A (2012): Local phosphocycling mediated by LOK/SLK restricts ezrin function to the apical aspect of epithelial cells. J Cell Biol 199:969–984.
65. Viswanatha R, Bretscher A, Garbett D (2014): Dynamics of ezrin and EBP50 in regulating microvilli on the apical aspect of epithelial cells. Biochem Soc Trans 42:189–194.
66. Santello M, Toni N, Volterra A (2019): Astrocyte function from information processing to cognition and cognitive impairment. Nat Neurosci 22:154–166.
67. Perea G, Navarrete M, Araque A (2009): Tripartite synapses: Astrocytes process and control synaptic information. Trends Neurosci 32:421–431.
68. Theodosis DT, Poulain DA, Oliet SHR (2008): Activity-dependent structural and functional plasticity of astrocyte-neuron interactions. Physiol Rev 88:983–1008.
69. Huang AY-S, Woo J, Sardar D, Lozzi B, Bosquez Huerta NA, Lin C-CJ, *et al.* (2020): Region-specific transcriptional control of astrocyte function oversees local circuit activities. Neuron 106:992–1008.e9.
70. Kullmann DM, Min MY, Asztely F, Rusakov DA (1999): Extracellular glutamate diffusion determines the occupancy of glutamate receptors at CA1 synapses in the hippocampus. Philos Trans R Soc Lond B Biol Sci 354:395–402.
71. Lozovaya NA, Kopanitsa MV, Boychuk YA, Krishtal OA (1999): Enhancement of glutamate release uncovers spillover-mediated transmission by N-methyl-d-aspartate receptors in the rat hippocampus. Neuroscience 91:1321–1330.
72. Scanziani M, Salin PA, Vogt KE, Malenka RC, Nicoll RA (1997): Use-dependent increases in glutamate concentration activate presynaptic metabotropic glutamate receptors. Nature 385:630–634.
73. Mitchell SJ, Silver RA (2000): Glutamate spillover suppresses inhibition by activating presynaptic mGluRs. Nature 404:498–502.
74. Ireland DR, Abraham WC (2002): Group I mGluRs increase excitability of hippocampal CA1 pyramidal neurons by a PLC-independent mechanism. J Neurophysiol 88:107–116.
75. Piet R, Vargová L, Syková E, Poulain DA, Oliet SHR (2004): Physiological contribution of the astrocytic environment of neurons to intersynaptic crosstalk. Proc Natl Acad Sci U S A 101:2151–2155.
76. Parpura V, Heneka MT, Montana V, Oliet SHR, Schousboe A, Haydon PG, *et al.* (2012): Glial cells in (patho)physiology. J Neurochem 121:4–27.